PHYSICAL REVIEW B **103**, L060402 (2021)

Letter

Distinct magnetic ground states of R_2ZnIrO_6 (R=La, Nd) determined by neutron powder diffraction

H. Guo,[1,*] C. Ritter,[2] Y. Su,[3] A. C. Komarek,[4] and J. S. Gardner[1]

[1]*Neutron Science Platform, Songshan Lake Materials Laboratory, Dongguan, Guangdong 523808, China*
[2]*Institut Laue-Langevin, Boite Postale 156X, F-38042 Grenoble Cedex 9, France*
[3]*Jülich Centre for Neutron Science, Heinz Maier-Leibnitz Zentrum, Forschungszentrum Jülich, Lichtenbergstrasse 1, D-85747 Garching, Germany*
[4]*Max Planck Institute for Chemical Physics of Solids, Nöthnitzer Strasse 40, D-01187 Dresden, Germany*

(Received 17 December 2020; accepted 1 February 2021; published 12 February 2021)

Double-perovskite iridates A_2ZnIrO_6 (A=alkaline or lanthanide) show complex magnetic behaviors ranging from weak ferromagnetism to successive antiferromagnetic transitions. Here we report the static (dc) and dynamic (ac) magnetic susceptibility and neutron powder diffraction measurements for A=La and Nd compounds to elucidate the magnetic ground state. Below 10 K, the A=La compound is best described as canted iridium moments in an antiferromagnet arrangement with a propagation vector $\mathbf{k} = 0$ and a net ferromagnetic component along the c axis. On the other hand, Nd_2ZnIrO_6 is described well as an antiferromagnet with a propagation vector $\mathbf{k} = (\frac{1}{2}\frac{1}{2}0)$ below $T_N \sim 17$ K. Scattering from both the Nd and Ir magnetic sublattices was required to describe the data, and both were found to lie almost completely within the ab plane. The dc susceptibility revealed a bifurcation between the zero-field-cooled and field-cooled curves below ~13 K in Nd_2ZnIrO_6. A glassy state was ruled out by ac susceptibility but detailed magnetic isotherms revealed the opening of the loop below 13 K. These results suggest a delicate balance exists between the Dzyaloshinskii-Moriya, crystal field schemes, and d-f interaction in this series of compounds.

DOI: 10.1103/PhysRevB.103.L060402

A double perovskite with the general formula $A_2B'B''O_6$ forms an ordered rocksaltlike structure when the B' and B'' ions are physically and/or chemically significantly different. In general, the A site is occupied by an alkaline or lanthanide cation, and B'/B'' are transition-metal elements. This structure is incredibly versatile, hosting a wide variety of ions on the A, B', and B'' sites. The interplay between crystal structure, orbital and spin degrees of freedom, and electron-lattice coupling leads to a diverse range of physical properties from metal-insulator transition [1] to multiferroicity [2] and a large magnetoresistance effect [3] to photolysis [4]. For a single magnetic B'-/B''-site compound, the superexchange coupling between two nearest cations through intermediate oxygen takes part in the magnetic order. Generally, when the A site is occupied by a magnetic cation, the trivalent lanthanide orders at a lower temperature than the transition-metal sublattice [5,6]. Recently, double perovskites with Ir ions at the B'' site have attracted much attention [5,7–13] due to the relatively large spin-orbit coupling (SOC) of the Ir^{4+} ion, which may lead to novel phenomena such as the SOC-driven Mott insulator [14] and complex magnetism [15–17]. Some $A_2B'IrO_6$ have been synthesized, but the magnetic ground states are still not well understood. La_2MgIrO_6 shows antiferromagnetic behavior below $T_N = 12$ K [7]. Isovalent substitution of Zn for Mg results in a different magnetic ground state, where the magnetic susceptibility increases substantially below 10 K and hysteresis is observed in magnetic isothermals below this temperature, suggesting a ferromagnetic component to the magnetic structure [7]. More recent studies on small single crystals suggested a canted antiferromagnetic state with a net moment along the crystallographic b axis [18]. Introducing rare-earth moments on the A site gives rise to complex magnetic properties [12], and in Nd_2ZnIrO_6 two transitions have been observed in the magnetic susceptibility below ~17 K. Preliminary neutron powder diffraction (NPD) measurements exist for these compounds, but a reliable model to explain the materials with two magnetic sublattices has so far eluded scientists. The relatively large neutron absorption by Ir ions and their comparatively small magnetic moment limit the statistics and reduce the uniqueness of models.

In this paper, we perform NPD measurements, as well as bulk dc and ac magnetic susceptibility measurements on polycrystalline La_2ZnIrO_6 and Nd_2ZnIrO_6, in order to investigate the static magnetic ground state. La_2ZnIrO_6 forms a canted antiferromagnetic structure where the moments are constrained within the bc plane with a finite ferromagnetic component along the long c axis. This result differs from the earlier neutron diffraction and first-principles calculations that did not detect a ferromagnetic component [7]. Our results are similar to, but also inconsistent with, the single-crystal magnetization data that found the easy axis along the crystallographic b axis [18]. Substituting the nonmagnetic La^{3+} with the magnetic Nd^{3+}, we found long-range antiferromagnetic order below 17 K in Nd_2ZnIrO_6. Data at 1.8 K are described well as an antiferromagnet with the moments (Nd and Ir) lying almost exactly within the ab plane and with no net moment. Interestingly, only one transition was detected

---

[*] hjguo@sslab.org.cn

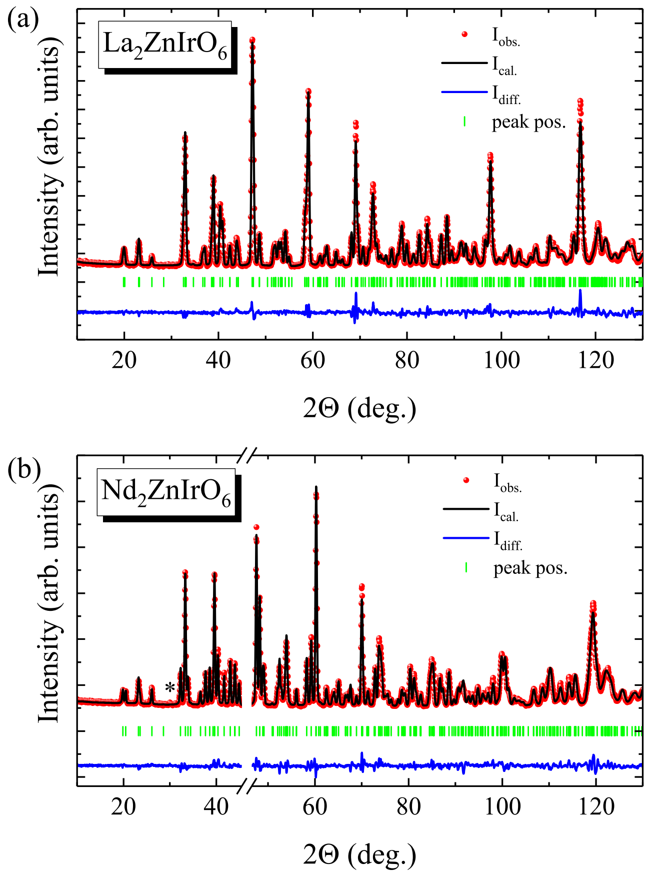

FIG. 1. Rietveld refined patterns from R_2ZnIrO_6. These high-resolution data were collected at room temperature on the D2B diffractometer. The lattice parameters are $a = 5.5906(2)$ Å, $b = 5.6871(2)$ Å, $c = 7.9312(2)$ Å, $\beta = 90.00(1)^\circ$ for (a) the $R =$ La sample and $a = 5.4697(2)$ Å, $b = 5.7313(2)$ Å, $c = 7.8058(2)$ Å, $\beta = 89.97(1)^\circ$ for (b) the $R =$ Nd sample. A small peak originating from the cryofurnace has been excluded from the refinement in (b), and the asterisk marks the peak originating from the $Nd_2Ir_2O_7$ phase.

in both NPD and ac susceptibility measurements at $T_N \sim 17$ K, while two are seen in the bulk static susceptibility. The distinct ground states of these two double perovskites reveal the delicate balance between the Dzyaloshinskii-Moriya interaction and *d-f* superexchange interaction within these compounds.

Polycrystalline samples of La_2ZnIrO_6 and Nd_2ZnIrO_6 were prepared by the solid-state reaction method. Stoichiometric amounts of raw materials of La_2O_3, Nd_2O_3, ZnO, and IrO_2 were mixed and ground thoroughly in an agate mortar. The powders were then pressed into pellets and sintered between 900 °C and 1100 °C in air for about 20 days with several intermediate grindings. Phase purity was checked by x-ray diffraction (XRD) and NPD measurements. Magnetization measurements were performed using the vibrating sample magnetometer (MPMS3, Quantum Design). The ac susceptibility was measured in a physical property measurement system (Quantum Design) with an ac excitation field of 5 Oe. NPD measurements were performed at the Institut Laue-Langevin (ILL) in Grenoble, France. High-*Q*-resolution measurements, for crystal structure determination, were performed on the D2B diffractometer with 1.594-Å neutrons selected by a Ge(335) monochromator, while the D20 diffractometer produced a higher flux beam of 2.394-Å neutrons, albeit with lower resolution suitable for magnetic structure refinements. Approximately 7 g of samples were loaded into annular vanadium cans to reduce the neutron flight path within the sample, overcoming the high neutron absorption from naturally abundant Ir. The La_2ZnIrO_6 sample was measured on the D20 diffractometer for 10.25 h at 20 and 1.8 K. Due to the stronger magnetic signal from the Nd_2ZnIrO_6 sample, 2-h measurements at 1.8, 13.5, 15.1, and 19.3 K, were performed. In addition, a series of 15-min measurements were carried out while ramping the temperature at 0.1 K/200 s and 0.1 K/450 s between 1.8–12 and 12–20 K, respectively. These data allowed the temperature dependence of the magnetic peak intensities to be determined, which is proportional to the magnetization squared. To determine the magnetic contribution to the NPD, a high-temperature (paramagnetic) data set was subtracted from that collected at lower temperatures. Rietveld refinements were performed using the FULLPROF software suite [19] together with SARAH for symmetry analysis [20].

Both XRD and NPD measurements indicate an impurity-free phase for the La_2ZnIrO_6 sample, but a small amount of $Nd_2Ir_2O_7$ (about 0.1 wt %) was found in the Nd_2ZnIrO_6 sample. Refinement of the crystal structure confirms both samples crystallize into a monoclinic structure with space group $P2_1/n$ (No. 14; see Fig. 1). In addition, NPD measurements were able to investigate the presence of *B*-site disorder. In La_2ZnIrO_6, this amounts to between 6(4)% from the D2B measurement and 13(4)% from the D20 measurement, as will be discussed later. Similar antisite disorder was found to be negligible in Nd_2ZnIrO_6.

The temperature dependence of the magnetic susceptibility and isothermal magnetization measurements are shown in Fig. 2. For La_2ZnIrO_6, the magnetic susceptibility increases abruptly below 10 K, concomitant with a splitting between the zero-field-cooled (ZFC) and field-cooled (FC) magnetization curves and hysteresis in the isothermal magnetization loop, suggesting a weak ferromagnetic component in the ground state. On the other hand, the Nd_2ZnIrO_6 sample shows a more complicated path to the ground state. A broad peak can be found at 17 K below which long-range antiferromagnetic order is observed, but a second magnetic phase is revealed in the splitting between the ZFC and FC magnetization curves below 13 K. Note that the magnitude of the susceptibility in Nd_2ZnIrO_6 is much smaller than that of the La_2ZnIrO_6 sample, although the net magnetic moment is larger [see Figs. 2(a2) and 2(b2)] due to the much larger Nd^{3+} moment. These bulk results are consistent with those reported in the literature [7,12]. The temperature dependence of the real component of the dynamic susceptibility of Nd_2ZnIrO_6 is shown in the inset of Fig. 2(b1) when measured in a zero dc field. These data reveal no dependence on excitation frequency excluding a possible spin-glass-like origin of the 13 K anomaly in the static magnetization similar to that seen in the double perovskite La_2CoIrO_6 by Song *et al.* [21]. In order to study the magnetic phase below 13 K further, careful

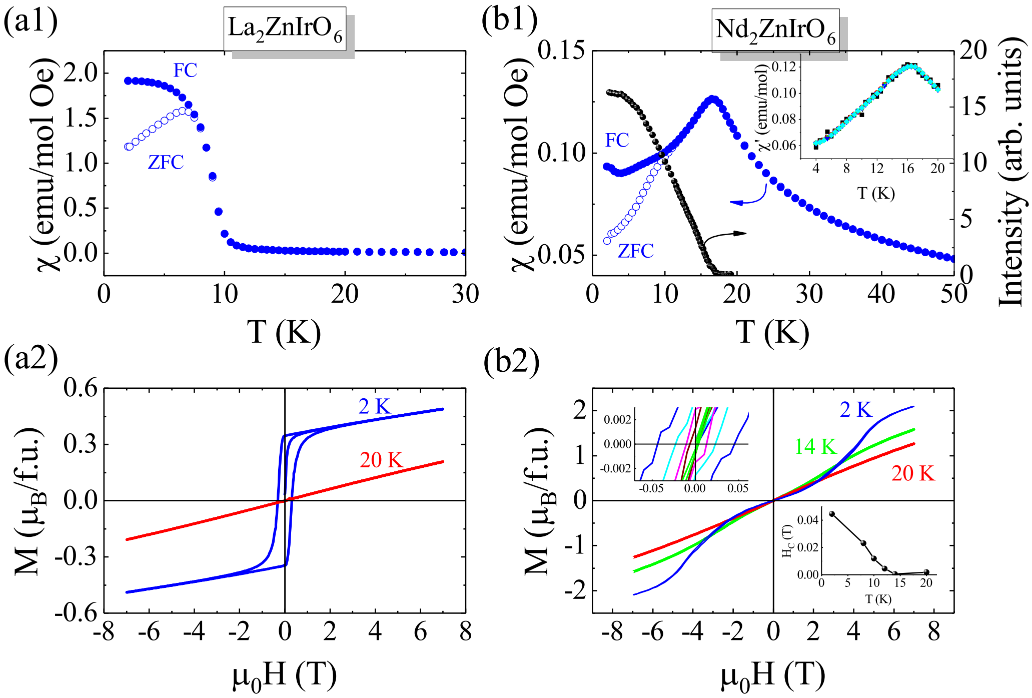

FIG. 2. Temperature dependence of the magnetic susceptibility and isothermal magnetization measurements for (a1) and (a2) La$_2$ZnIrO$_6$ and (b1) and (b2) Nd$_2$ZnIrO$_6$. The susceptibility was measured with a field of 1000 Oe. The temperature dependence of the magnetic peak intensity, measured on D20, is also shown in (b1), where the 13 K transition is absent. The inset in (b1) shows the real component χ' of the zero-field ac susceptibility with frequencies of 13, 113, 1333, 5330, and 9918 Hz. The top inset in (b2) is an enlargement of the low-field region measured at 2 K (blue), 8 K (cyan), 10 K (magenta), 12 K (wine), and 14 K (green). The bottom inset shows the temperature dependence of the coercive field H_c.

magnetic isotherms were collected around this temperature up to 7 T. Unlike La$_2$ZnIrO$_6$ [Fig. 2(a2)], in which an antiferromagnet develops a ferromagnetic component and a loop opens up around the origin below the critical temperature, in Nd$_2$ZnIrO$_6$ below the high-temperature transition no gap is seen in the magnetization loops, consistent with a simple antiferromagnet. However, below the second transition at 13 K, the loops take on a S shape, typical of a metamagnet, and on closer inspection [top inset in Fig. 2(b2)] a small gap opens up around the origin, suggestive of a ferromagnetic component to the ordering, similar to that in La$_2$ZnIrO$_6$.

In order to determine the underlying magnetic structures for both compounds, we have performed NPD measurements on the high-flux D20 diffractometer at the ILL in the absence of a magnetic field. Atomic structure refinements were performed at 20 K in the paramagnetic state, allowing the scale factors to be determined and fixed for subsequent magnetic structure refinements. All measurements were performed after cooling in zero field. We first concentrate on the La$_2$ZnIrO$_6$ sample, where the magnetic peaks can be indexed with a $\mathbf{k} = 0$ propagation vector using the K-SEARCH program. These data and the magnetic structure refinements confirmed the Zn/Ir mixing (B-site disorder) previously observed in the crystallographic data collected on D2B. Magnetic symmetry analysis of the Ir1 moment (2c site) and the cation-disordered Ir2 moment on the Zn position (2d site) with the monoclinic space group $P2_1/n$ shows that the reducible magnetic representation is decomposed into two irreducible representations (IRs) as $\Gamma = \Gamma_1 + \Gamma_3$. The basis vectors (BVs) for each IR can be found in the Supplemental Material (SM) in Table S1 [22]. The magnetic intensities can be well described by the IR Γ_3. As can be seen from Fig. 3, a B-site ordered model results in a poorer fit and R_B value compared to the B-site disordered model. Note that in order to have the same magnitude of magnetic moment at the Ir1 and Ir2 atoms, the degree of disorder obtained from the magnetic refinement is ∼13(4)%, which is slightly larger than the 6(4)% found from the D2B refinement. The obtained magnetic structure is shown in Figs. 4(a) and 4(b). The magnitude of the moment is $0.87\mu_\mathrm{B}$/Ir at 1.8 K, and the Ir moments are lying predominately within the bc plane with $\mu_b = 0.403(7)\mu_\mathrm{B}$ and $\mu_c = 0.773(8)\mu_\mathrm{B}$ at B'' and $\mu_b = 0.30(5)\mu_\mathrm{B}$ and $\mu_c = 0.82(5)\mu_\mathrm{B}$ for the Ir that has accidentally substituted for Zn on the B' site. As can be seen, there is a canting of these spins resulting in a net moment along the c axis, which explains the ferromagnetic component observed by bulk magnetic susceptibility measurements [see Fig. 2(a2) at base temperature]. Single-crystal magnetization measurements led Han *et al.* to conclude that the b axis was the easy axis [18], which would correspond to the IR Γ_1. However, the IR Γ_1 does not describe our neutron data (see Fig. S1 in the SM [22]). Also incompatible with our data, Cao *et al.* suggested that the moments lie within the ab plane by local-density approximation + U calculations [7], which need to be revisited in light of our conclusions.

As mentioned above, the static magnetic susceptibility suggests a different magnetic ground state for Nd$_2$ZnIrO$_6$ compared to La$_2$ZnIrO$_6$. Additional magnetic peaks can be observed below $T_\mathrm{N} \sim 17$ K, which can be indexed with a

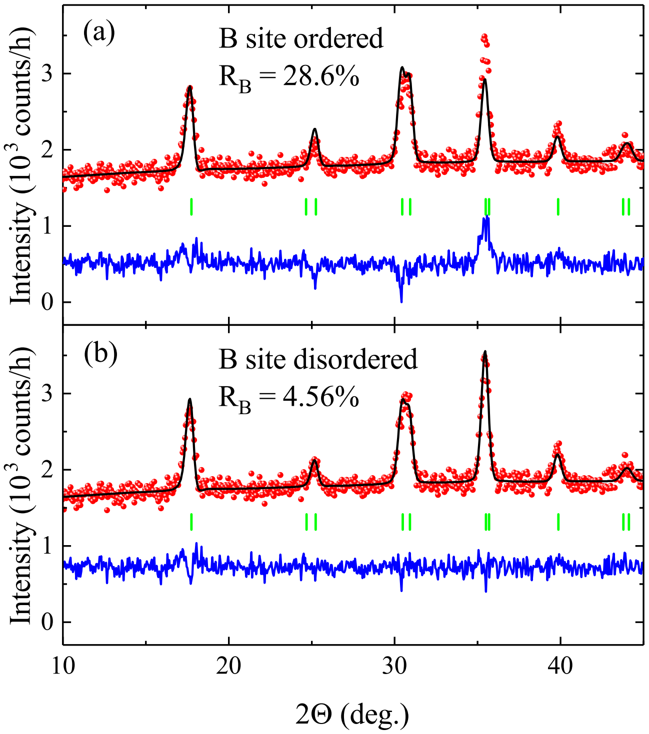

FIG. 3. Rietveld refinement of the magnetic diffraction from La_2ZnIrO_6 at 1.8 K. A paramagnetic data set, taken at 20 K, has been subtracted to remove the scattering from the crystal lattice. The calculated patterns are according to the IR Γ_3 with (a) a perfectly ordered *B*-site model and (b) a *B*-site disordered model where the best model found 13(4)% site substitution between Zn and Ir ions. Red dots: experimental data; black curve: calculated data; vertical bars: magnetic peak position; blue curve: difference between the experimental and calculated data.

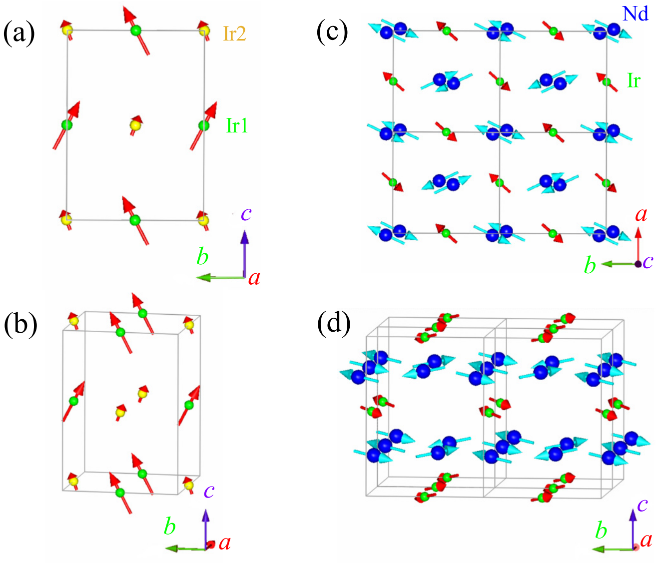

FIG. 4. Magnetic structure of (a) and (b) La_2ZnIrO_6 and (c) and (d) Nd_2ZnIrO_6 viewed along different directions. The Ir moments have been enlarged for clarity. Note that the smaller Ir2 moments in (a) and (b) are visualized taking into account the partial occupation effect.

propagation vector $\mathbf{k} = (\frac{1}{2}\frac{1}{2}0)$, consistent with an earlier report [12]. The temperature dependence of the integrated peak intensity at $2\Theta \sim 25.1^\circ$ monotonically increases as the temperature is lowered through T_N, and no anomaly is seen at 13 K, where bulk magnetic susceptibility reveals a splitting of the ZFC and FC curves [see Fig. 2(b1)].

Symmetry analysis of the Nd ions at the 4*e* site and Ir ions at the 2*c* site with the propagation vector $k = (\frac{1}{2}\frac{1}{2}0)$ shows that the reducible magnetic representations decompose as follows:

$$\Gamma_{\mathrm{Ir}} = \Gamma_1 + \Gamma_3, \tag{1}$$

$$\Gamma_{\mathrm{Nd}} = \Gamma_1 + \Gamma_2 + \Gamma_3 + \Gamma_4. \tag{2}$$

The corresponding BVs are listed in SM Tables S2 and S3 [22]. As pointed out by an earlier report [12], half of the magnetic moments are not ordered for either of these IRs, and a combination of the two IRs is required in order to form a fully ordered state. In addition, if a coupling exists between the two magnetic sublattices and the magnetic transition is second order in character [23], both sublattices should order under the same IR. An earlier report [12] determined the ordering of the Nd^{3+} moments, but Vogl *et al.* were not able to resolve the ordering of the Ir^{4+} moments due to insufficient statistics. Using the high-flux diffractometer, D20, at the ILL, we are able to solve the magnetic structure of this compound, which must include static moments on both the Nd and Ir sublattices to describe the data well. Consistent with the high-resolution neutron diffraction data, no antisite disorder was required to describe these data.

As can be seen from SM Table S2 [22], only one solution, i.e., $\Gamma_1 + \Gamma_3$, is possible. The best refinements with Nd and Ir sublattices ordering under $\Gamma_1 + \Gamma_3$ are shown in Fig. 5. Focusing on the low-intensity peaks in the right panels of Fig. 5, it is clear that a model with only the Nd sublattice ordering cannot account for the peak intensities around $2\Theta \sim 40^\circ$. This is more apparent close to T_N, where the sizes of both the Nd and Ir moments are expected to be small and comparable, producing a more significant interference effect, as observed in the pyrochlore iridate $Nd_2Ir_2O_7$ [16]. The refined magnetic moments at 1.8 K are listed in Table I, and the magnetic structure is shown in Figs. 4(c) and 4(d). The moments for both Nd and Ir ions prefer to lie within the *ab* plane, in contrast to the La_2ZnIrO_6 case.

The value of the Nd moment is much smaller than the free-ion value ($g_J = 8/11$, $J = 9/2$), presumably due to the crystal electric field effect, as observed in similar compounds [24]. It can be seen in Table I that although both magnetic sublattices develop concomitantly, the Nd moment at 15.1 K (2 K below the transition temperature) is only 39% of that at 1.8 K, while the Ir moment is already 72% of the low-temperature value by 15.1 K. This observation suggests the Ir sublattice is the driving force of the magnetic ordering. The obtained antiferromagnetic structure has zero net moment along any crystallographic direction; thus, the origin of the weak ferromagnetic component seen in static magnetic susceptibility and FC/ZFC splitting measurements is still a puzzle. This bulk susceptibility character seems to be ubiquitous in the iridates. The pyrochlore iridates show all-in/all-out magnetic

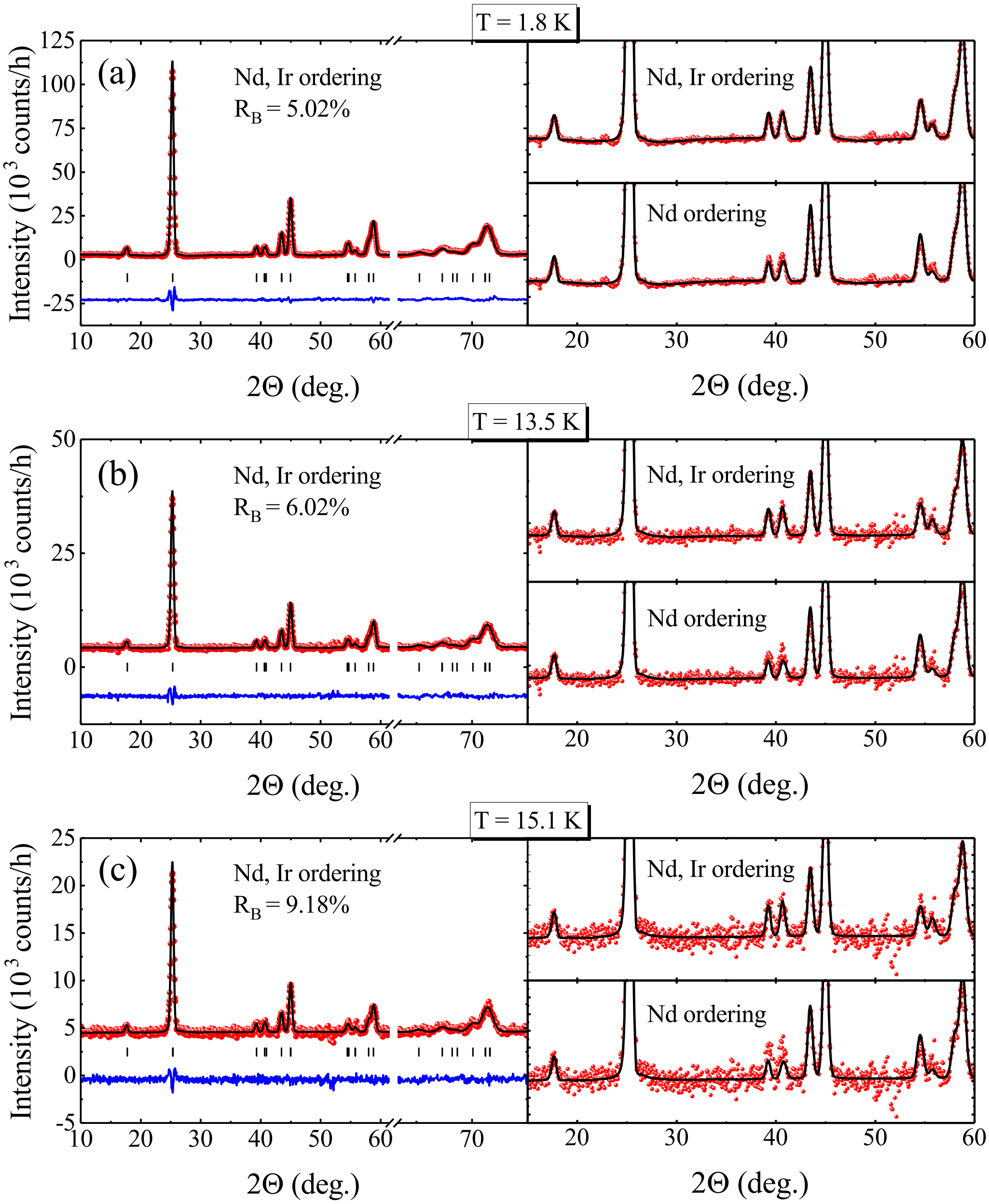

FIG. 5. Rietveld magnetic refinement of the difference pattern at various temperatures for Nd_2ZnIrO_6 according to IR $\Gamma_1 + \Gamma_3$. The left panels show the refinement results with perfectly ordered Nd and Ir sublattices, and the right panels highlight an expanded region of low peak intensities, comparing our best model and that with only the Nd sublattice ordering. Red dots: experimental data; black curve: calculated data; vertical bars: magnetic peak position; blue curve: difference between the experimental and calculated data. A small angular range around $2\Theta = 62^\circ$ was excluded from the fits due to contamination from the atomic scattering that did not subtract well.

structure with zero net moment, whereas the static magnetic susceptibility also shows the bifurcation below T_N and was attributed to the formation of antiferromagnetic domain walls [25–27]. One difference is that the bifurcation occurs at T_N for the pyrochlore iridate, while it appears at lower temperature for Nd_2ZnIrO_6. Another possibility is a subtle change in the magnetic symmetry at this temperature, which could result in a small net moment; this was not detected in our current study but may require higher-resolution, single-crystal magnetic structural refinement studies. The former scenario would correspond to a phase separation, while the latter would occur within one phase. Future studies using a local probe would be helpful to elucidate this point.

To conclude we have determined with the aid of neutron powder diffraction and symmetry analysis the long-range magnetic structure of La_2ZnIrO_6, albeit with approximately $\frac{1}{8}$ disorder on the B site. This simple $\mathbf{k} = 0$ structure has a net moment along the c axis. Further studies are needed to elucidate the role of site disorder in these findings. Adding Nd^{3+} with a magnetic moment to the rare-earth site results in a significant change in the chemistry and bulk magnetic properties. No crystallographic disorder was found in this sample,

TABLE I. Moment size for the Nd and Ir ions at different temperatures according to the best refinement assuming both sublattices order under the same IR $\Gamma_1 + \Gamma_3$. The unit of the moment is μ_B.

		1.8 K	13.5 K	15.1 K
Nd	μ_a	0.94(2)	0.47(2)	0.27(3)
	μ_b	1.98(1)	1.10(1)	0.78(1)
	μ_c	0.38(7)	0.24(4)	0.24(4)
	$\|\mu\|$	2.23(2)	1.22(1)	0.87(2)
Ir	μ_a	−0.47(5)	−0.41(4)	−0.37(5)
	μ_b	−0.53(4)	−0.40(3)	−0.36(3)
	μ_c	0.15(4)	0.10(3)	0.08(4)
	$\|\mu\|$	0.72(4)	0.58(4)	0.52(4)

and all moments are predominantly in the *ab* plane. The iridium sublattice was found to drive the magnetic transition, but the 5*d*-4*f* interactions are clearly important, increasing the ordering temperature by 70%. Moreover, the single-ion anisotropy of the Nd^{3+} ion probably govern the spin direction, in this case rotating the preferred plane from the *bc* plane to the *ab* plane.

Double perovskites have been shown to be an excellent playground to investigate the interplay of spin-lattice and electron degrees of freedom. With the wide array of chemical diversity many double perovskites have also been shown to be technologically relevant. We hope this study motivates others to study Ir^{4+}-based double perovskites where spin-orbit coupling, on-site Coulomb interaction, and crystal field energies are of comparable energy. For example, in Nd_2ZnIrO_6 the isothermal magnetization curve at 2 K has the signature of a metamagnetic transition at about 2 T which should be studied in more detail, but this is true for many of the iridate-based double perovskites [5].

[1] H. Kato, T. Okuda, Y. Okimoto, Y. Tomioka, K. Oikawa, T. Kamiyama, and Y. Tokura, Phys. Rev. B **65**, 144404 (2002).

[2] Y. Shimakawa, M. Azuma, and N. Ichikawa, Materials **4**, 153 (2011).

[3] K. I. Kobayashi, T. Kimura, H. Sawada, K. Terakura, and Y. Tokura, Nature (London) **395**, 677 (1998).

[4] J. Luo, J.-H. Im, M. T. Mayer, M. Schreier, M. K. Nazeeruddin, N.-G. Park, S. D. Tilley, H. J. Fan, and M. Grätzel, Science **345**, 1593 (2014).

[5] X. Ding, B. Gao, E. Krenkel, C. Dawson, J. C. Eckert, S.-W. Cheong, and V. Zapf, Phys. Rev. B **99**, 014438 (2019).

[6] J. Sánchez-Benítez, M. J. Martínez-Lope, J. A. Alonso, and J. L. García-Muñoz, J. Phys.: Condens. Matter **23**, 226001 (2011).

[7] G. Cao, A. Subedi, S. Calder, J. Q. Yan, J. Yi, Z. Gai, L. Poudel, D. J. Singh, M. D. Lumsden, A. D. Christianson, B. C. Sales, and D. Mandrus, Phys. Rev. B **87**, 155136 (2013).

[8] W. K. Zhu, C.-K. Lu, W. Tong, J. M. Wang, H. D. Zhou, and S. X. Zhang, Phys. Rev. B **91**, 144408 (2015).

[9] A. A. Aczel, A. M. Cook, T. J. Williams, S. Calder, A. D. Christianson, G. X. Cao, D. Mandrus, Y.-B. Kim, and A. Paramekanti, Phys. Rev. B **93**, 214426 (2016).

[10] M. Vogl, L. T. Corredor, T. Dey, R. Morrow, F. Scaravaggi, A. U. B. Wolter, S. Aswartham, S. Wurmehl, and B. Büchner, Phys. Rev. B **97**, 035155 (2018).

[11] B. Singh, M. Vogl, S. Wurmehl, S. Aswartham, B. Büchner, and P. Kumar, Phys. Rev. Research **2**, 023162 (2020).

[12] M. Vogl, R. Morrow, A. A. Aczel, R. B. Rodriguez, A. U. B. Wolter, S. Wurmehl, S. Aswartham, and B. Büchner, Phys. Rev. Mater. **4**, 054413 (2020).

[13] Y. Gao, Z. Tian, L. Xu, M. Ashtar, Z. Wan, Z. Xia, F. Yang, S. Yuan, Y. Han, and W. Tong, J. Phys.: Condens. Matter **32**, 465802 (2020).

[14] B. J. Kim, H. Jin, S. J. Moon, J. Y. Kim, B. G. Park, C. S. Leem, J. Yu, T. W. Noh, C. Kim, S. J. Oh, J. H. Park, V. Durairaj, G. Cao, and E. Rotenberg, Phys. Rev. Lett. **101**, 076402 (2008).

[15] H. Guo, K. Matsuhira, I. Kawasaki, M. Wakeshima, Y. Hinatsu, I. Watanabe, and Z.-a. Xu, Phys. Rev. B **88**, 060411(R) (2013).

[16] H. Guo, C. Ritter, and A. C. Komarek, Phys. Rev. B **94**, 161102(R) (2016).

[17] H. Guo, C. Ritter, and A. C. Komarek, Phys. Rev. B **96**, 144415 (2017).

[18] H. Han, W. Liu, Y. Dai, Y. Gao, Z. Tian, J. Fan, S. Zhou, L. Pi, C. Zhang, L. Zhang, and Y. Zhang, Phys. Rev. B **98**, 054403 (2018).

[19] J. Rodríguez-Carvajal, Phys. B (Amsterdam, Neth.) **192**, 55 (1993).

[20] A. Wills, Phys. B (Amsterdam, Neth.) **276–278**, 680 (2000).

[21] J. Song, B. Zhao, L. Yin, Y. Qin, J. Zhou, D. Wang, W. Song, and Y. Sun, Dalton Trans. **46**, 11691 (2017).

[22] See Supplemental Material at http://link.aps.org/supplemental/10.1103/PhysRevB.103.L060402 for the basis vectors for each IR and the refinement based on the IR Γ_1 for La_2ZnIrO_6.

[23] E. Bertaut, Acta Crystallogr. **24**, 217 (1968).

[24] A. A. Aczel, D. E. Bugaris, J. Yeon, C. de la Cruz, H.-C. zur Loye, and S. E. Nagler, Phys. Rev. B **88**, 014413 (2013).

[25] K. Matsuhira, M. Wakeshima, Y. Hinatsu, and S. Takagi, J. Phys. Soc. Jpn. **80**, 094701 (2011).

[26] E. Y. Ma, Y.-T. Cui, K. Ueda, S. Tang, K. Chen, N. Tamura, P. M. Wu, J. Fujioka, Y. Tokura, and Z.-X. Shen, Science **350**, 538 (2015).

[27] H. T. Hirose, J.-i. Yamaura, and Z. Hiroi, Sci. Rep. **7**, 42440 (2017).